Temperature dependence of photoconversion efficiency in silicon heterojunction solar cells: Theory vs experiment

A. V. Sachenko,[1] Yu. V. Kryuchenko,[1] V. P. Kostylyov,[1] A. V. Bobyl,[2] E. I. Terukov,[2,3] S. N. Abolmasov,[3] A. S. Abramov,[3] D. A. Andronikov,[3] M. Z. Shvarts,[2] I. O. Sokolovskyi,[1] and M. Evstigneev[4,a)]
[1]*V. Lashkaryov Institute of Semiconductor Physics, NAS of Ukraine, 41 prospect Nauky, 03028 Kyiv, Ukraine*
[2]*Ioffe Institute, 194021 St.-Petersburg, Russian Federation*
[3]*TFTC Ioffe R&D Center, 194021 St.-Petersburg, Russian Federation*
[4]*Department of Physics and Physical Oceanography, Memorial University of Newfoundland, St. John's, Newfoundland and Labrador A1B 3X7, Canada*

(Received 28 January 2016; accepted 24 May 2016; published online 8 June 2016)

Silicon heterojunction solar cells (HJSC) with the efficiency of about 20% are manufactured. Their short-circuit current, open-circuit voltage, photoconversion efficiency, and fill factor of the current–voltage curve are measured in a broad temperature range from 80 to 420 K. It is established that the open-circuit voltage, the fill factor, and the photoconversion efficiency are non-monotonic functions of temperature, having a maximum in the vicinity of 200 K. A new approach to modeling of HJSCs is proposed, which allows one to obtain quantitative agreement with the experimental results at temperatures above 200 K, as well as to describe the results published in the literature on the solar cells under AM1.5 conditions. The temperature coefficient of photoconversion efficiency in HJSCs is discussed, and its low value is shown to be related to the low surface and volume recombination rates. Finally, a theoretical expression for the SC's temperature under natural working conditions is derived. *Published by AIP Publishing.* [http://dx.doi.org/10.1063/1.4953384]

I. INTRODUCTION

Recently, there has been a substantial progress in increasing the photoconversion efficiency of the silicon heterojunction solar cells (HJSC), see Refs. 1 and 2 for a state-of-the-art review. For instance, Masuko *et al.*[3] reported the efficiency of 25.6% under standard conditions (AM1.5 G spectrum, 1000 W/m^2 incident power density). According to the estimates performed in several works, such as Refs. 4 and 5, the highest theoretical efficiency of silicon-based photoconverters under unfocused solar radiation is about 30%. In order to approach the limit efficiency, it is necessary to intensify the research aiming at optimizing the parameters of these structures. This requires deeper understanding of the peculiarities of the processes that take place in silicon HJSCs as compared to the standard ones.

The principal difference between the HJSCs and the p-n junction-based ones is that in the former, in order to contribute to the photoinduced current, the photogenerated electrons and holes need to travel through the wide-bandgap layers. Typically, these are the layers of α-Si:H.[2] However, in a view papers, other materials are used, such as α-SiC:H[6] and α-SiO$_x$:H.[7] The band diagram of a heterojunction depends both on the bandgaps of the semiconductors in contact and on the respective electron affinities. The absence of a barrier on the heterojunction boundary for at least one band is not a rule, but an exception. In the case considered, the very thin layers of α-Si:H, whose bandgap exceeds the bandgap of Si by at least 0.5 eV, behave as dielectrics. The current transport through such layers proceeds via either direct or multistep trap-assisted tunneling.[8] As estimates show, the former mechanism cannot produce the transfer of photogenerated electrons and holes for dielectric thicknesses of the order of 10 nm, the typical thickness of the α-Si:H layers in HJSCs. Therefore, the photocurrent through the α-Si:H layers is most likely due to the trap-assisted tunneling.

This work reports the results of our experimental and theoretical investigation of HJSCs' principal characteristics—short-circuit current density, J_{SC}; open-circuit voltage, V_{OC}; current–voltage curve fill factor, FF; and photoconversion efficiency, η—obtained in a broad temperature range from 80 to 420 K. We are aware of only a few studies published in the literature, where the temperature dependence of these parameters in HJSCs is reported. However, the temperature interval probed in those works is much narrower than in our experiment, from the room temperature to T not exceeding 150 K above the room temperature.[7,9,10] In Ref. 11, the dark I–V curves were measured in an interval from 100 to 400 K. Finally, Schulze *et al.*[12] performed these measurements under illumination conditions, probing the interval from 240 K to 360 K. In the present work, we found that at lower temperatures, the output power, open-circuit voltage, and fill factor develop a maximum at about 200 K. We introduce a semianalytical model of the temperature dependences measured, allowing one to obtain quantitative agreement with the experiment at temperatures above 200 K.

We note that the analogous theoretical studies that we are aware of usually employ numerical simulations of, e.g., the package AFORS-HET, and do not contain direct comparison with the experiment.[13–15] In particular, their findings

a)Author to whom correspondence should be addressed. Electronic mail: mevstigneev@mun.ca

cannot be employed to explain our experimental results, because they were obtained for a fixed temperature $T = 298$ K under AM1.5 G irradiation conditions.

In our theoretical treatment, we derive the conditions, under which the determination of the photoconversion efficiency η in the HJSCs can be performed using the same procedure as in usual p-n junction-based solar cells. The model presented here takes into account the distinct features of the HJSCs as compared to the conventional solar cells. In the first place, these features are related to the high bulk Shockley–Hall–Read lifetime $\tau_{SHR} \geq 1$ ms. Due to this, the inequalities $\Delta p \geq N_d$ and $L \gg d$ hold in a broad temperature range, where Δp is the excess electron–hole density in the base region (Si single crystal), N_d is the doping level, L is the diffusion length of the minority carriers in the base, and d is the base thickness. We show that for $\Delta p \geq N_d$, the open-circuit voltage V_{OC} is higher than in the standard case $\Delta p < N_d$ not only because of the higher Δp-value but also because of the additional contribution due to the back surface of the solar cell.

We take into account several recombination mechanisms. We establish that in HJSC solar cells at $T > 200$ K, Shockley–Hall–Read and surface recombination dominate at relatively low base doping level, whereas interband Auger recombination dominates at high base doping level. We explain the notable insensitivity of the HJSCs' photoconversion efficiency to temperature as compared to the commercial solar cells.[16,17] First and foremost, by the essential reduction of the total bulk and surface recombination rates in the HJSCs.

In order to explain the experimental temperature dependence of the fill factor and photoconversion power, we take into account the increase of the series resistance in the low-temperature range, which is due to the increase of the contact resistance. Also, experimental measurement of the shunt resistance yielded the rather high value of about $7 \times 10^4\ \Omega$, allowing us to neglect its effect in the modeling.

Finally, by means of solving the equations for photogenerated current and voltage coupled to the temperature balance equation, we find the temperature of HJSC under working conditions. We show that a solar cell operating under the AM0 radiation conditions in the environment with the temperature of about 173 K (–100 °C) has the temperature exceeding 300 K. The reason is insufficient radiative cooling, which, in turn, is related to the fact that about 80% of the solar energy incident on the HJSCs is converted into heat. Under the AM1.5 conditions, cooling down of the solar cells is due to radiation and convection, as a result of which the temperature of the solar cell notably decreases. However, apart from the cases of high wind velocity, the temperature of the solar cells under natural conditions exceeds the environment temperature by about 10 °C.

II. FABRICATION AND CHARACTERIZATION OF HETEROJUNCTION SOLAR CELLS

The structure of the Si-HJSC used in this study is shown in Fig. 1. It contains a textured single-crystal n-type silicon substrate of (100) orientation, produced by Czochralski

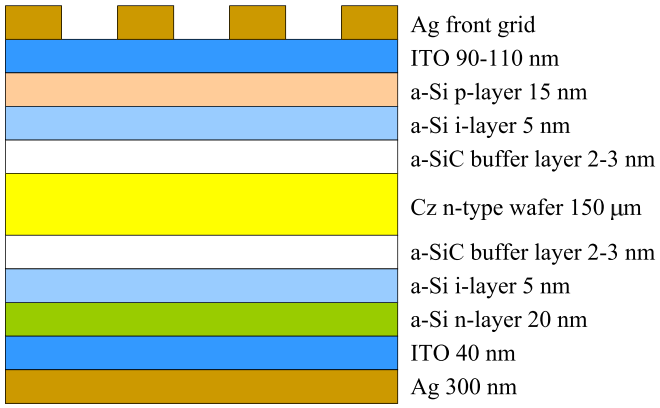

FIG. 1. Schematic illustration of Si-HJSC used in this study; surface texture is not shown.

method (Cz). It has the doping level $N_d \approx 10^{15}\ \text{cm}^{-3}$, thickness $d \approx 150$ μm, and Shockley–Hall–Read lifetime of charge carriers $\tau_{SHR} \approx 1$ ms. On its front side, we deposited a buffer α-SiC layer followed by layers of intrinsic amorphous silicon α-Si, p-type α-Si, transparent conducting indium tin oxide (ITO), and a silver grid that collects current. On the rear side is a buffer layer, followed by intrinsic α-Si, n-type α-Si, ITO, and silver layers. All α-Si:H layers were produced in a Gen5 ($110 \times 140\ \text{cm}^2$) plasma enhanced chemical vapor deposition (PECVD) reactor, whereas ITO and Ag layers were deposited using a magnetron sputtering system.[18] The buffer films ensured suppression of the epitaxial film growth at the α-Si:H/c-Si interface. The thickness of these layers is about 2–3 nm. The parameters of our Si-HJ solar cells are indicated in Table I. The last fabrication step was deposition of a solid contact film on the back side and contact grid on the front side of the solar cell. The photoactive surface area of the cell, including the contact grid, was $A = 4.34\ \text{cm}^2$.

In order to facilitate absorption of the incident radiation by the semiconductor bulk on both sides of the substrate, we created microtextures in the form of randomly located vertical pyramids with characteristic size of a few micrometers. In Ref. 3, it was shown that such surface morphology allows one to obtain the short-circuit current density J_{SC} of $41.8\ \text{mA/cm}^2$ under AM1.5 conditions. Estimates that account for shadowing of the solar cell by the contact grid indicate that, in this case, the external quantum yield is close to 96%, whereas the internal quantum yield of the photogenerated current is close to 100%.

III. THEORETICAL FORMULATION

The mathematical description of photoconversion processes in HJSCs is similar to the already solved problem of photoconversion efficiency in structures consisting of a conducting layer, a tunneling layer of SiO_2, and a layer of Si, where the majority carriers (electrons) enter the metal via thermionic emission, and the minority carriers (holes) tunnel through the dielectric layer.[8] In HJSCs, both electrons and holes tunnel through the thin dielectric layer. In order to be able to treat the nanometer layers on the front and the rear sides of the HJSC as dielectrics, light absorption and electron–hole pair generation in these layers must be weak. This

TABLE I. Parameters of our HJSC. J_{SC}, V_{OC}, and η are given for $T = 300$ K.

N_d (cm^{-3})	d (μm)	τ_b (ms)	J_{SC} (mA/cm^2)	V_{OC} (V)	S (cm/s)	η (%)	R_{S0} (Ω)	A_t ($\mu\Omega$)	φ_c (V)	E_{00} (meV)
10^{15}	150	1	36.54	0.682	25	18.4	0.2	0.4	0.39	23

condition holds very well for the rear layer, because the energy of the photons reaching it is much smaller than the bandgap energy. With respect to the front one, before reaching it, light has to travel through the relatively thick (about 100 nm) ITO layer, where the most energetic photons are absorbed. For the remaining low-energy photons, the product of the absorption coefficient and the α-Si:H layer thickness is much smaller than 1, so that they are practically not absorbed by α-Si:H. In that case, by introducing the phenomenological tunneling coefficients for electrons and holes, it is possible to write down the criteria, under which the transport through these layers occurs without losses, and the open-circuit voltage is practically unaffected by α-Si:H. These coefficients can be calculated, e.g., using the AFORS-HET package.

Taking into account tunneling through the wide-bandgap layers and the fact that the density of surface states is extremely small, the boundary conditions for the electron and hole current densities, J_n and J_p, in the case of non-degenerate semiconductor read:

$$J_p = q\frac{V_p}{4}\theta_p[p(x) - p_0(x)]_{x=0}\,,$$
$$J_n = q\frac{V_n}{4}\theta_n[n(x) - n_0(x)]_{x=d}\,. \tag{1}$$

Here, q is the elementary charge, V_p and V_n are the mean thermal velocities of holes and electrons, respectively, θ_p and θ_n are their tunneling coefficients, $p(x)$ and $n(x)$ are the densities of electrons and holes, and $p_0(x)$ and $n_0(x)$ are the respective equilibrium densities. In the second expression, d is the thickness of Si layer.

As shown in Ref. 8, the minority carriers' current (for definiteness, we assume these to be holes) is collected without recombination losses if the condition

$$V_{pe} = \frac{V_p\theta_p}{4}e^{-y(0)} \gg V_r + S, \tag{2}$$

is fulfilled, where V_{pe} is the effective hole emission rate from the semiconductor into the metal, $y(0)$ is the nonequilibrium electrostatic potential (band bending) normalized to k_BT/q in the $x = 0$ plane, V_r and S are, respectively, bulk and surface recombination rates. The inequality (2) should hold not only in the short-circuit regime but also in the regime of maximal power. Estimates obtained for the typical parameter values of the HJSCs indicate that (2) is fulfilled for $\theta_p \geq 10^{-5}$, which is the case in our HJSCs.

The dependence of the short-circuit current on temperature is due to the temperature dependence of the bandgap and absorption coefficient.[19] It can be expressed as

$$J_{SC}(T) = q\int_{\lambda_0}^{\lambda_m(T)} d\lambda\, Q_e(\lambda, T)\,\Phi(\lambda)\,\frac{\lambda}{hc}\,, \tag{3}$$

where $\lambda_m(T) = hc/E_g(T) \approx 1.24\,\mu\text{m eV/E}_g\text{(T)}$ is the photoelectric threshold in Si, λ_0 is the absorption edge, $Q_e(\lambda, T)$ is the external quantum efficiency of the cell, and $\Phi(\lambda)$ is the spectral density of the incident radiation. The temperature dependence of the bandgap in Si can be found, e.g., in Ref. 20. The increase of $J_{SC}(T)$ with temperature is due to the variations of both $\lambda_m(T)$ and $Q_e(\lambda, T)$ with T. Because the latter dependence is difficult to determine theoretically, we use, instead of Eq. (3), an empirical expression, which approximates the product $Q_e\Phi$ in the integrand of (3) by a black-body spectrum:

$$J_{SC}(T) = J_{SC}(300\,\text{K})\,\frac{F(T)}{F(300\,\text{K})}, \tag{4}$$

where

$$F(T) = \int_0^{\lambda_m(T)} \frac{d\lambda}{\lambda^4\left(e^{hc/\left(kT_{eff}\lambda\right)} - 1\right)}\,. \tag{5}$$

In general, the effective temperature T_{eff} is smaller than the radiation temperature T_L. However, under the AM0 conditions, or when an incandescent lamp is used, the two temperatures are practically the same, provided that the quantum efficiency is close to 1.

For the open-circuit voltage in HJSCs, the following general expression applies:

$$V_{OC} = \frac{k_BT}{q}\Big(\big(\Delta y_{OC}(0) - \Delta y_{SC}(0)\big) - \big(\Delta y_{OC}(d) - \Delta y_{SC}(d)\big)\Big), \tag{6}$$

where $\Delta y_{OC}(0)$ and $\Delta y_{SC}(0)$ are the dimensionless variations of the band bending in the open-circuit and short-circuit regimes, respectively, at $x = 0$, and $\Delta y_{OC}(d)$ and $\Delta y_{SC}(d)$ are the respective values at $x = d$.

Our estimates indicate that in HJSCs that completely conduct the current generated in the short-circuit regime, the following conditions hold: $\Delta y_{SC}(0) \ll 1$ and $-\Delta y_{SC}(d) \ll 1$ (see the Appendix). Therefore, in this case, the value of V_{OC} is practically the same as in the standard p-n junction-based solar cells. Taking into account that $p_0n_0 = n_i^2$, where n_i is the intrinsic charge carrier density, the open-circuit voltage is

$$V_{OC} \approx V_{OC1} + V_{OC2}, \quad V_{OC1} = \frac{kT}{q}\ln\frac{\Delta p_0 n_0}{n_i^2}$$
$$V_{OC2} = \frac{kT}{q}\ln\left(1 + \frac{\Delta p_0}{n_0}\right), \tag{7}$$

where Δp_0 is the excess electron–hole pair density in the Si bulk in the open-circuit regime. The expression (7) for V_{OC} is valid when the moduli of band bending at $x = 0$ and $x = d$

in the absence of illumination exceed the respective values in the open-circuit regime,

$$y_0(0) > qV_{OC1}/kT, \quad y_0(d) > qV_{OC2}/kT\,. \tag{8}$$

Usually, these inequalities are well satisfied in HJSCs, at least at the operating temperatures.

Eq. (7) is a quadratic equation for Δp_0 with the solution

$$\Delta p_0 = -\frac{n_0}{2} + \sqrt{\frac{n_0^2}{4} + n_i^2 e^{qV_{OC}/k_BT}}\,. \tag{9}$$

The open-circuit voltage can be found from the balance equation relating the short-circuit current and the recombination currents due to the Shockley–Hall–Read mechanism with the characteristic time τ_{SHR}, radiative recombination with the time τ_r, Auger recombination with the rate R_{Auger}, surface recombination with the rate S, and recombination in the space-charge region with rate R_{SC}:

$$J_{SC} = q[d(\tau_{SHR}^{-1} + \tau_r^{-1}) + R_{Auger} + S + R_{SC}]\Delta p_0, \tag{10}$$

where[21,22]

$$\begin{aligned} R_{Auger} &= C_p(n_0 + \Delta p_0)\Delta p_0 + C_n(n_0 + \Delta p_0)^2\,, \\ C_p &= 10^{-31}\,\mathrm{cm^6/s}\,, \\ C_n &= \left(2.8\cdot 10^{-31} + \frac{2.5\cdot 10^{-22}}{(n_0+\Delta p_0)^{0.5}}\right)\mathrm{cm^6/s}\,. \end{aligned} \tag{11}$$

The space-charge region recombination rate is given by[23]

$$R_{SC}(\Delta p_0) \approx \frac{L_D}{\tau_{SHR}}\int_{y_{pn}}^{-0.1} dy \frac{n_0+\Delta p_0}{\sqrt{e^y - y - 1}} \times \left[(n_0+\Delta p_0)e^y + n_i(T)e^{\varepsilon_r} + b\left(\frac{n_i(T)^2}{n_0+\Delta p_0} + \Delta p_0\right)e^{-y} + n_i(T)e^{-\varepsilon_r}\right]^{-1}, \tag{12}$$

where $L_D = \sqrt{\varepsilon_0\varepsilon_S kT/(2q^2 n_0)}$ is the Debye screening length, ε_0 is the relative dielectric constant of the semiconductor, $b = \sigma_p/\sigma_n$ is the ratio of the capture cross-sections of a hole and an electron by a deep recombination center, $\varepsilon_r = E_r/kT$ is the normalized energy of the deep recombination level measured from the middle of the band gap, y is the dimensionless potential, and y_{pn} is the dimensionless potential at the p-n junction boundary.

The intrinsic charge carrier density in Si is given by the empirical expression[20]

$$n_i(T) = 5.71\cdot 10^{19}\left(\frac{T}{300\,\mathrm{K}}\right)^{2.365} e^{-6773\,\mathrm{K}/T}\,\mathrm{cm^{-3}}, \tag{13}$$

and the equilibrium electron density can be obtained from the relations $n_0 = p_0 + N_d$, $p_0 n_0 = n_i^2$:

$$n_0 = \frac{N_d}{2} + \sqrt{\frac{N_d^2}{4} + n_i^2}, \tag{14}$$

where N_d is the donor density.

As our estimates using the parameters from Table I have shown that, in the temperature range from 200 K to 300 K, Δp_0 is about $5 \times 10^{15}\,\mathrm{cm^{-3}}$, and R_{SC} does not exceed 0.1 cm/s. Thus, the space-charge region recombination rate is insignificant in comparison to the total bulk and surface recombination.

The fill factor, FF, can be written as

$$FF = \frac{J_m V_m}{J_{SC} V_{OC}}\left(1 - \frac{R_S J_m A}{V_m}\right), \tag{15}$$

where J_m and V_m are the photoinduced current density and voltage in the maximum-power regime, A is the surface area, and R_S is the series resistance of the solar cell.

To determine J_m and V_m of a HJSC, one has to consider the current–voltage relation [cf. Eq. (10)]

$$J(V) = J_{SC} - q(d(\tau_{SHR}^{-1} + \tau_r^{-1}) + R_{Auger} + S)\,\Delta p(V), \tag{16}$$

where

$$\Delta p(V) = -\frac{n_0}{2} + \sqrt{\frac{n_0^2}{4} + n_i^2 e^{qV/k_BT}}. \tag{17}$$

The maximum power condition $d(VI(V))/dV = 0$ yields the value of V_m, whose substitution into (16) allows one to determine J_m.

Another approach to this problem can be based on the two-diode model.[12] We do not use this model, because it describes the dark current–voltage curves. In our work, we use the light I–V measurements, neglecting tunneling current and current in the space-charge region. The reason for this neglect is that under the maximum-power conditions ($V_m = 580\,\mathrm{mV}$), and especially in the open-circuit regime ($V_{OC} = 682\,\mathrm{mV}$), their contribution is small. At the same time, the salient feature of our approach is that, in the current–voltage characteristics, we take into account not only the front but also the rear side of the cell. In the language of the two-diode model this means that in the limiting case when the excess electron–hole pair density Δn is much greater than the equilibrium density n_0 in the base region, the I–V curve with the ideality factor 2 is realized, whereas in the opposite limit, the ideality factor is 1, see Ref. 24.

The total series resistance R_S consists of the bulk resistance of the material, R_{bS}, sheet resistance R_{SS} of the ITO film used as a transparent conductor, and contact resistance R_{CS}. The first two contributions to series resistance are usually temperature-independent. The temperature dependence of the contact resistance is determined by the nature of the current transport mechanism through the contact. If the current is due to thermionic or field emission, R_{CS} increases on cooling. The resistance R_{CS} is presumably related to the resistance of ITO-metal contact. Because the ITO film is degenerate, we can expect that the current transport through the contact is due to the field emission mechanism. Then, the expression for the series resistance can be written as[25]

$$R_S = R_{S0} + A_t(T)\exp\left(\frac{q\phi_C}{E_{00}\coth(E_{00}/k_BT)}\right), \tag{18}$$

where R_{S0} is the temperature-independent component of the series resistance, $A_t(T)$ is the prefactor that depends on temperature according to a power law, ϕ_C is the contact barrier

height, and E_{00} is the characteristic electron tunneling energy in the semiconductor. If the barrier ϕ_C is sufficiently high, then one can neglect the temperature dependence of the prefactor.

The photogenerated power can be found from the standard expression

$$P = J_{SC} A V_{OC} FF \tag{19}$$

and the photoconversion efficiency is given by

$$\eta = \frac{P}{AP_S}, \tag{20}$$

where $P_S = 1000\,\mathrm{W/m^2}$ is the surface power density of the incident radiation and $A = 4.34\,\mathrm{cm^2}$ is the surface area of the sample.

IV. COMPARISON BETWEEN THE THEORETICAL AND EXPERIMENTAL CHARACTERISTICS OF HETEROJUNCTION SOLAR CELLS

In the measurements of the HJSC current–voltage curves, we used a simulator of solar radiation (Yamashita Denso Corp., Model SS-80AA, class AAA) that produces illumination of $1\,\mathrm{kW/m^2}$ with the AM1.5 G spectrum for the irradiation region of $30\,\mathrm{mm} \times 30\,\mathrm{mm}$. The light coming from this source was directed by an optical collimation system to a quartz window (diameter 50 mm) of a vacuum chamber, in which the SC was placed. The chamber contained a vertical cryostat (model VPF-100, Janis Research) with a cryogenic temperature controller (Model 325, Lake Shore Cryotronics, Inc.), which allowed us to perform temperature measurements in the range 80–400 K and enabled temperature stability of 1 K. The chamber was evacuated with a HiCube 80 Eco pump (Pfeiffer Vacuum) down to 10^{-4} mBar. The current–voltage recording system consisted of a bipolar voltage source Kepco BOP 36–12, a reference resistor of $0.1\,\Omega$ (Burster GmbH, model 1282–0.1, precision 0.02%), and two multimeters Keithley 2000, which measured the voltage across the HJSC and across the reference resistor. To determine and control the illuminance in the sample plane, we used a standard World Photovoltaic Scale SC calibrated at the Fraunhofer Institute for Solar Energy Systems as in Ref. 26. The calibration of the photoinduced current in our samples at $T = 298\,\mathrm{K}$ was performed under direct illumination from the solar simulator using a thermally stabilized base with a Peltier element, a temperature controller based on the Eurotherm 2216e unit (Eurotherm Co.) with a temperature detector RTD-100 (Omega, U.S.A.).

For the sample placed inside the vacuum chamber, the photoinduced current measured at the calibration stage was used as an indicator of the correct value of the incident radiation power to compensate for a small loss of irradiation energy in the collimation block and in the quartz window. Outside of the chamber, a control photocollector was placed in order to monitor the stability of the irradiation intensity during the measurements of the temperature dependence of HJSC's characteristics.

After having set the required photocurrent in the SC, corresponding to the irradiation power density of $1000\,\mathrm{W/m^2}$, the sample was cooled down to 80 K under constant irradiation from the solar imitator. In this way, we could compensate for the small warming up of the sample due to irradiation, and to ensure a good agreement between the real temperature of the SC and its measured value. The *I–V* curve and the photoelectric parameters (J_{SC}, V_{OC}, FF, and P_{max}) were measured on heating the sample.

Fig. 2 shows the short-circuit current vs. temperature curve. The theoretical curve was produced by fitting the experimental data points with Eq. (4); the best fit was achieved for the effective temperature $T_{eff} = 4030\,\mathrm{K}$. The agreement of the experimental and the theoretical curve in the whole temperature range is obvious.

Fig. 3 shows the temperature dependence of the open-circuit voltage, $V_{OC}(T)$. The theoretical curves are obtained by numerically solving Eq. (10) supplemented by Eqs. (11) and (4) with parameters from Table I. When building these curves, we used the temperature-dependent $J_{SC}(T)$, and the intrinsic carrier density $n_i(T)$ given by Eq. (13). We neglected the temperature dependence of the Shockley–Hall–Read, radiative, surface, and Auger recombination rates, because they are much weaker than the $n_i(T)$ dependence. It is noteworthy that for the equilibrium electron densities $n_0 \simeq 10^{15}\,\mathrm{cm^{-3}}$, which correspond to the doping level, interband Auger recombination and radiative recombination can be neglected in comparison to the bulk Shockley–Hall–Read and surface recombination. Auger recombination becomes essential when $n_0 \geq 10^{16}\,\mathrm{cm^{-3}}$.

As can be seen in Fig. 3, the theoretical curve agrees well with the experimental results at $T \geq 180\,\mathrm{K}$. The temperature coefficient of $V_{OC}(T)$ at $T > 200\,\mathrm{K}$ is about 1.8 mV/K, which is close to the typical value of $|dV_{OC}/dT| \approx 2\,\mathrm{mV/K}$ in the industrial silicon-based solar cells with diffused p-n junctions. At temperatures below 180 K, the experimental and theoretical values of $V_{OC}(T)$ deviate from each other: the theoretical open-circuit voltage increases, whereas the experimental one decreases on cooling. Finding possible reasons for experimentally observed non-monotonic $V_{OC}(T)$ behavior is a complicated problem. First of all, as follows

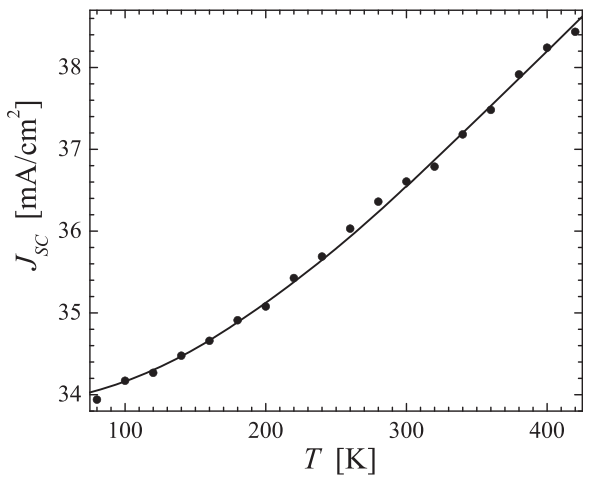

FIG. 2. Experimental (circles) and theoretical (line) temperature dependence of the short-circuit current.

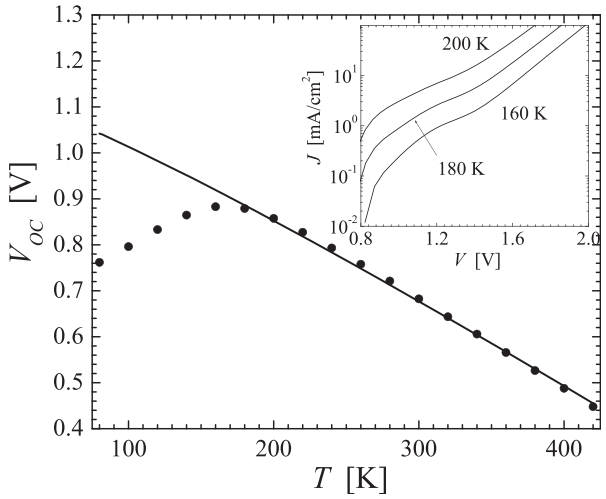

FIG. 3. Experimental (circles) and theoretical (lines) temperature dependence of the open-circuit voltage obtained using the general expression (10) with parameters shown in Table I. The inset shows the current–voltage curves at three different temperatures in the low-temperature range.

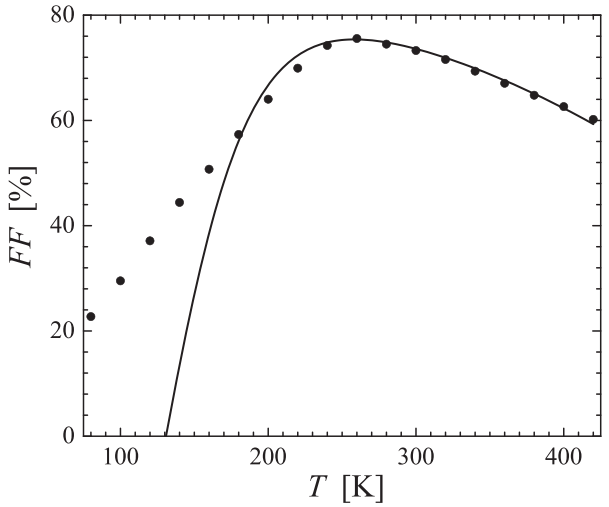

FIG. 4. Experimental (circles) and theoretical (lines) temperature dependence of the current–voltage curve fill factor.

from the calculations based on the spectrum of localized donor-like and acceptor-like states in α-Si:H, this material is a heavily compensated semiconductor,[27] whose degree of compensation increases on reducing the temperature. Therefore, the charge in the acceptor-doped α-Si:H decreases on cooling, leading to the reduction of $y(x=0)$. This implies that although the criterion (2) at $T \leq 200$ K is fulfilled in the short-circuit regime, it breaks down at a relatively weaker bias. This point is illustrated by the experimental current–voltage curves of our HJSCs measured at $T = 200$, 180, and 160 K, see inset in Fig. 3. Similar to Ref. 28, these curves exhibit sections due to the hole tunneling from the narrow-band single-crystal Si into α-Si:H for relatively high direct bias ($\geq$1.4 V), whereas for weaker bias ($\leq$0.82 V), the dark current–voltage curves are adequately described by the expressions of the form (16) and (17) (with $J_{SC} = 0$). Thus, the reduction of $V_{OC}(T)$ on cooling is due to several reasons. It is the decrease of $y(x=0)$ and failure of the criterion (2), i.e., the reduction of the photogenerated current at low temperatures. As the value of $y(x=0)$ goes down on cooling, the inequality $kTy_0(x=0) > qV_{OC}$ breaks down, where $y_0(x=0)$ is the dimensionless band bending in the absence of illumination. Then, the expression (7) becomes inadequate, and the open-circuit voltage becomes smaller than the value predicted by (7). Finding a better formula for V_{OC} in the low-temperature range is a complicated task, which requires the knowledge of the distribution of the localized states in the doped and undoped layers of α-Si:H. Additional research is needed to attack this problem.

Fig. 4 shows the temperature dependence of the fill factor. It is seen that FF at low temperatures becomes anomalously low, signaling a strong increase of the series resistance R_S on cooling. The theoretical curve was obtained from Eqs. (15) and (18) for the same parameters as the theoretical curve $V_{OC}(T)$ from Fig. 3. We took $A_t = 4 \times 10^{-7}\,\Omega$, $\varphi_c = 0.387$ V, $E_{00} = 0.0225$ eV, and $R_{S0} = 0.2\,\Omega$. The agreement between the theoretical and the experiment curves is very good at $T \geq 200$ K, whereas at $T < 200$ K, the discrepancy between theory and experiment is observed for the reasons discussed above.

We note that the non-monotonic temperature dependence of the fill factor in HJSCs was observed in the work by Taguchi *et al.*[9] for the double and triple thicknesses of α-Si:H layers, and in the work by Seif *et al.*[7] for the case of α-SiO_x:H layers. This non-monotonicity was explained in Ref. 7, based on the work by Anderson,[30] by the fact that, at low temperatures, not all photogenerated current can pass through the wide-bandgap layer due to the band offset at the interface between c-Si and α-Si layers. In our case, the maximum of the $FF(T)$ curve is observed at a much lower temperature. For this reason, we believe it to be principally due to the temperature dependence of the contact resistance.

The temperature dependence of the photoconversion efficiency η, see Eq. (20), is shown in Fig. 5. The agreement between theory and experiment at $T \geq 200$ K, including its non-monotonic behavior, is obvious. Above about 280 K, the efficiency decreases approximately linearly with temperature. This linear decay can be described by an expression[16]

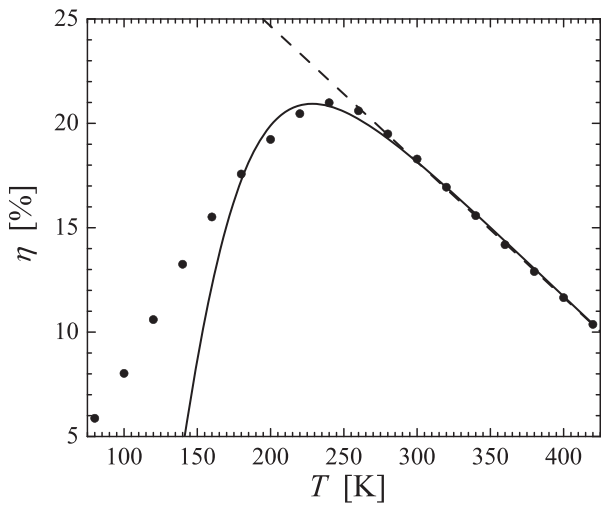

FIG. 5. Experimental (circles) and theoretical (lines) temperature dependence of the photoconversion efficiency.

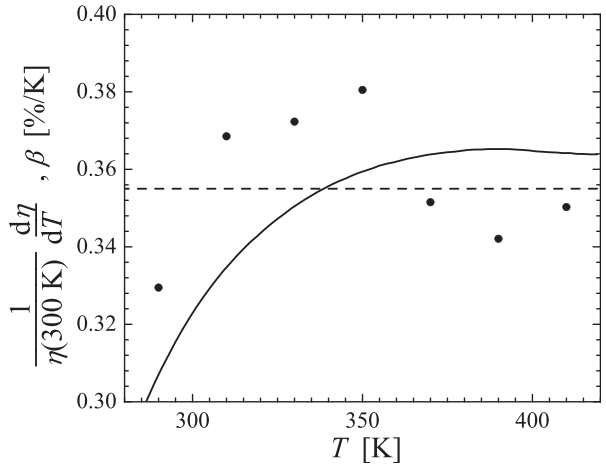

FIG. 6. Experimental (dashed line, circles) and theoretical (solid line) temperature dependence of the photoconversion power reduction coefficient. The dashed line was obtained by fitting the $P(T)$ curve, Fig. 5, at $T > 280\,\mathrm{K}$. The circles are obtained by numerically differentiating the experimental data using Eq. (22); the solid line is obtained from the derivative of the respective theoretical curve.

$$\eta(T) = \eta(300\,K)(1 - \beta(T - 300\,\mathrm{K})), \tag{21}$$

which defines the temperature coefficient β. A linear fit to the experimental data at $T \geq 280\,\mathrm{K}$ yields $\beta_{exp} = 0.355\%/\mathrm{K}$, see Fig. 5, dashed line. Theoretically, the photoconversion efficiency vs. temperature curve slightly deviates from the linearity (21), see the solid line in Fig. 6 showing the theoretical derivative of the efficiency with respect to temperature normalized to $\eta(300\,\mathrm{K})$ as well as the respective experimental estimates. To obtain the experimental curve based on the set of experimental support points (T_n, η_n), $n = 1, 2, \ldots$, we used the third-order accurate approximation for the derivative at the midpoint $T_{n+1/2} = (T_n + T_{n+1})/2$:

$$\frac{1}{\eta(300\,\mathrm{K})}\frac{d\eta}{dT}\left(T_{n+1/2}\right) \approx \frac{1}{\eta(300\,\mathrm{K})}\frac{\eta_{n+1} - \eta_n}{T_{n+1} - T_n}\,. \tag{22}$$

The overall trend towards saturation of both experimental and theoretical curves is clear, and the discrepancy between the two sets of data is due to the amplification of the experimental uncertainty by the derivative expression (22).

In the work,[17] the efficiency temperature coefficient in HJSCs with $\eta = 23\,\%$ was measured. Its value at the largest open-circuit voltage V_{OC} of 0.745 V, which was realized at the smallest solar cell thickness (see Fig. 3 of Ref. 17), was 0.23%/K. Our theoretical estimates at $T = 298\,\mathrm{K}$ and parameter values from Ref. 17, in the thickness range of the Si substrate from 80 to 165 μm, give $\beta \approx 0.25\%/\mathrm{K}$, quite close to the experimental values.

We note that the low values of $\beta(T)$ are directly related to the high excitation level in the open-circuit regime. This owes, in particular, to the minimal surface recombination rate in HJSCs. An important role here is played by atomic hydrogen, which leads to a strong reduction in the number of surface centers responsible for recombination. As shown in Ref. 31, it was precisely the use of atomic hydrogen that allowed obtaining minimal surface recombination rate of about 0.25 cm/s on Si.

The bulk recombination rate, $V_r = d/\tau_b$, where τ_b is the bulk lifetime, is also much smaller in HJSCs than in the diffused p-n junction-based solar cells. This is because, as shown above, HJSCs employ silicon with long Shockley–Hall–Read lifetimes exceeding 1 ms. Second, d in HJSCs is also smaller than in the usual solar cells. For instance, for $d = 100\,\mu$m and $\tau_{SHR} = 1\,\mathrm{ms}$, $V_r = 10\,\mathrm{cm/s}$. These features make it possible to maintain a high excitation level $\Delta p_0 \gg n_0$ in HJSCs, and thus to maximally reduce the temperature dependence of V_{OC} and η, and to minimize β.

The approach introduced in this work allows one to obtain the main characteristics of HJSCs under standard test conditions (AM1.5G, 1000 W/m^2). Table II shows the results of our calculations of V_{OC}, FF, and η for the parameters from Refs. 3, 17, and 29. These parameters include the doping level of $4.9 \times 10^{15}\,\mathrm{cm}^{-3}$, the lifetime in the base region equal to 3 ms, the SC thickness, and the experimental values of the short-circuit current. They were used to calculate the open-circuit voltage under AM1.5 conditions at the temperature 25 °C, using the expressions (9)–(11). In these equations, the surface recombination rate was treated as a fit parameter. As seen in Table II, in two cases out of three, the fit and the experimental values for the surface recombination rate are in very good agreement; in one case, the respective experimental value was not given in the original publication.[17]

Next, from the condition of maximum power, using Eqs. (16) and (17), the values of J_m and V_m were found, and then the fill factor was determined from Eq. (15). In this calculation, another fit parameter appears, namely, the series resistance. It can be determined uniquely by comparing the theoretical FF with the experimental value. Finally, the photoconversion efficiency is found using Eq. (20). As seen from Table II, the theoretical and experimental values agree with each other up to the fourth significant figure for all three SCs. With respect to the fill factor, the agreement between theory and experiment is slightly worse; however, the two sets of data do agree in three significant figures. In view of the empirical character of the short-current expression (4), we have used the experimental values of J_{SC} as the input parameters. The agreement between the theoretical and experimental results for V_{OC}, FF, and η demonstrates the correctness of the relations (10)–(20).

V. OPERATING TEMPERATURE OF A HETEROJUNCTION SOLAR CELL

In order to determine the solar cell's temperature in a realistic case, one needs to amend the equations for the photogenerated current and voltage by the energy balance equation. For the radiative cooling mechanism, this equation was obtained in Ref. 32. Taking the radiation and convection cooling mechanisms into account, it assumes the form:

$$P_S(1 - \varepsilon - \eta(T)) = aK_T\sigma(T^4 - T_S^4) + \gamma(T - T_S)\,. \tag{23}$$

Here, P_S is the power incident from the Sun, $\eta(T)$ is the conversion efficiency of the cell, and the parameter ε characterizes the energy dissipation due to radiative recombination. For silicon-based solar cells, where the Shockley–Hall–Read

TABLE II. Theoretical determination of V_{OC}, FF, and η for the systems studied in Refs. 3, 17, and 29. In all calculations, we have used the doping level $N_d = 4.9 \times 10^{15}\,\mathrm{cm}^{-1}$ and the Shockley–Hall–Read lifetime $\tau_{SHR} \approx 3$ ms. The thickness d and short-circuit current density J_{SC} are taken from the respective publications. Experimental values from Refs. 3, 17, and 29 are indicated in brackets.

Reference	d (μm)	S (cm/s)	J_{SC} (mA/cm^2)	V_{OC} (V)	FF (%)	η (%)	R_S (mΩ)
3	150	1.5 (1.5)	41.8	0.74 (0.74)	82.8 (82.7)	25.6 (25.6)	1.4
17	98	6	38.8	0.743 (0.743)	79.2 (79.1)	22.8 (22.8)	10
29	98	1.5 (<2)	39.5	0.75 (0.75)	83.4 (83.2)	24.7 (24.7)	1

lifetime, τ_{SHR}, as a rule, is much smaller than the radiative recombination time, τ_r, the value of the parameter ε is close to 0. The value of the parameter a, which depends on the grayness of the solar cell, i.e., on the closeness of the solar cell radiation spectrum to the black body spectrum, is also of the order of 1. The value of K_T equals the ratio of the HJSC's area that emits radiation to the area that receives radiation. The parameter σ is the Stefan–Boltzmann constant, $T = T_S + \Delta T$ is the temperature of the solar cell, and T_S is the environment temperature. Finally, γ is the convection coefficient, which depends on the magnitude and direction of the wind velocity, air humidity, and barometric pressure.[33]

Fig. 7 shows the results of the solution of Eqs. (20) and (23) under the standard AM1.5G conditions.

At high geographic latitudes, the main contribution to the yearly power yield of a solar plant comes from the time interval between spring and autumn, when the environment temperature is greater than 0 °C. The temperature of the solar cell is also positive. In this case, for the environment temperatures of 10, 20, and 30 °C, and $\gamma = 6 \times 10^{-3}$ W/cm^{2}K, the theoretical operating temperature of the HJSC exceeds the environment temperature by 11 °C, see Fig. 7.

For the AM0 conditions, typically realized when the solar cells are placed on a satellite, the environment temperature is about 173 K, see Ref. 34. Solution of Eqs. (20) and (23) with $\gamma = 0$ indicates that, in this case, because of the absence of convection mechanisms in the outer space, the working temperature of the solar cells is close to 49 °C.

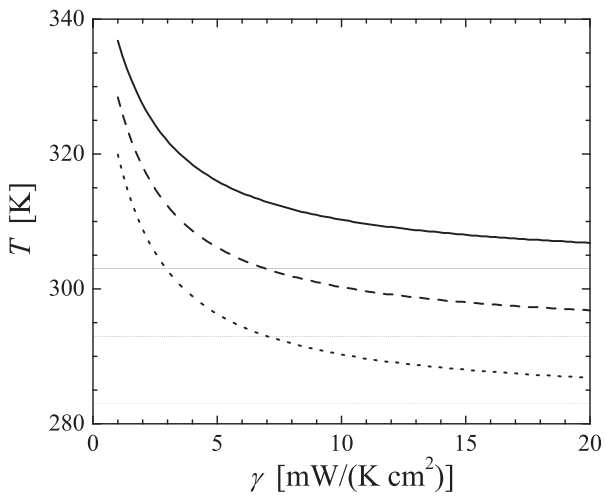

FIG. 7. Temperature of the HJSC vs. convection coefficient, γ. It is assumed that the surrounding temperature T_S is 30, 20, and 10 °C (from top to bottom curves). The horizontal lines correspond to the environment temperatures.

VI. CONCLUSIONS

Peculiarities of HJSC as opposed to the standard solar cells include, on the one hand, tunneling of electrons and holes through the α-Si:H layers; on the other hand, large number densities of the excess electron–hole pairs and large diffusion length of the minority charge carriers. In this work, we have derived the criteria, under which the tunneling processes do not lead to the deterioration of the HJSCs' characteristics as compared to those of the solar cells based on the diffused p-n junctions, and obtained the expressions for the main parameters that characterize the performance of HJSCs.

These expressions are compared to the experimental results. We have obtained good agreement between the theoretical and experimental temperature dependences of the HJSC parameters in the temperature range $T \geq 200$ K. At low temperatures, the series resistance, R_S, grows dramatically on cooling due to the contribution of the contact resistance. The reduction of the open-circuit voltage, V_{OC}, fill factor, FF, and photoconversion efficiency, η, at low temperatures is interesting from the scientific point of view. The reduction of FF and η is explained by the reduction of V_{OC} and by the increase of R_S. Of main practical interest are the results obtained for $T > 0$ °C. They are completely explained by the specifics of the HJSCs studies, especially the high excitation levels under AM1.5 conditions.

We have shown that the rather low value of the calculated temperature coefficient of photoconversion efficiency, $\beta(T) \approx 0.3\%$/K, near room temperature is in agreement with the data from Ref. 17. The physical reason of its low values in HJSC solar cells is low surface and bulk recombination rate as compared to the silicon diffused p-n junction-based solar cells.

The practical importance of these findings lies in the fact of their applicability in the analysis of HJSCs' performance under extreme temperature conditions realized, e.g., in the Earth polar regions, as well as in the outer space. In particular, high temperatures are realized, e.g., on the orbits of Venus, whereas low temperatures are found on the orbits of those planets which are far away from the Sun, such as Jupiter.

ACKNOWLEDGMENTS

This work was performed under the project of Minobrnauka RF No. 14.607.21.0075 (RFMEFI60714X0075). M.E. is grateful to the Natural Sciences and Engineering Research Council of Canada (NSERC) and to the Research and Development Corporation of Newfoundland and Labrador

(RDC) for financial support. Last but not least, we thank the anonymous Referees for their constructive input.

APPENDIX: JUSTIFICATION OF THE CONDITIONS $\Delta y_{SC}(0) \ll 1$, $|\Delta y_{SC}(d)| \ll 1$

Fig. 8 shows the dependence of V_{pe} on θ_p in the maximal power regime at $T = 300$ K. When building these plots, we took into account that the dimensionless band bending in the $x = 0$ plane is lower than the equilibrium value, i.e., $y(0) = y_0(0) - qV_m/k_BT$, where $V_m = 0.65$ V is the photogenerated voltage in the maximal-power regime. We have taken three values of the parameter $p_0(0) = p_0\, e^{-y_0(0)}$ of 10^{17}, 10^{18}, and $10^{19}\,\mathrm{cm}^{-3}$. For all these values, conductivity inversion in Si is realized near the boundary at $x = 0$, i.e., a charge-induced p-n junction is formed in the p-Si:H layer, which is necessary for normal functioning of the solar cell. The value of $p_0 = 10^5\,\mathrm{cm}^{-3}$ was taken, which corresponds to the doping level of $n_0 = 10^{15}\,\mathrm{cm}^{-3}$. The total value of $S + V_r$ was taken to be 50 cm/s. As seen in Fig. 8, the minimal value of V_{pe} equal to $S + V_r$ is realized at $\theta_p = 10^{-6}$ for $p_0(0) = 10^{17}\,\mathrm{cm}^{-3}$. For $\theta_p \geq 10^{-5}$, V_{pe} notably exceeds $S + V_r$ for all three values of $p_0(0)$ tested, i.e., the criterion (2) is well fulfilled.

In the Si case, the quasi Fermi levels of holes and electrons in the space-charge regions near the surface are, as a rule, constant. For non-degenerate semiconductors, the relations hold:

$$p = (p_0 + \Delta p)e^{-y(0)}\,,\quad n = (n_0 + \Delta p)e^{y(d)}, \tag{A1}$$

where p_0 and n_0 are the equilibrium electron and hole densities, and Δp is the excess electron–hole pair density in the Si neutral region.

Here, and in the following, we assume that the electron–hole pair diffusion length in HJSCs is much greater than the thickness of Si wafer, $L = \sqrt{D_p \tau_b} \gg d$ (D_p is the hole diffusion coefficient and τ_b is the lifetime). Because of this, Δp is the same at all x.

In the short-circuit regime

$$J_p = J_n = J_{SC}, \tag{A2}$$

where J_{SC} is the short-circuit current density. Substitution of the expressions (1) into this identity shows that the reduction of the coefficients τ_p and τ_n leads to the increase of the difference between the electron and hole densities on the contacts, $p(0) - p(d)$ and $n(0) - n(d)$, inversely proportionally to θ_n and θ_p. The estimates for $J_{SC} = 40\,\mathrm{mA/cm}^2$ indicate that for $\theta_{p,n} = 10^{-5}$, these differences are about $10^{16}\,\mathrm{cm}^{-3}$. Although this is a rather high value, it is substantially smaller than the equilibrium densities n_0 and p_0. This is called the accumulation effect, first pointed out in Ref. 35. Due to the accumulation effect, upon turning the illumination on, the short-circuit current saturates over the time scale necessary for the build-up of the difference $p(0) - p_0(0))$, at which the tunneling current becomes equal to the generation current.

We note that the relation (A2) and the expression

$$\Delta p_{SC} = \frac{J_{SC}}{qV_{pe}}, \tag{A3}$$

which is valid under the criterion (2) in the short-circuit regime, allow one to find the dimensionless bend bending in the $x = 0$ plane, $\Delta y_{SC}(0)$. In particular, if $\Delta y_{SC}(0) \ll 1$, we have

$$\Delta y_{SC}(0) = \frac{J_{SC}}{qp_0(0)\left(V_p\theta_p/4\right)}\,. \tag{A4}$$

Fig. 9 shows $\Delta y_{SC}(0)$ as a function of θ_p at different values of $p_0(0)$. As seen in this figure, for $\theta_p > 10^{-6}$, the inequality $\Delta y_{SC}(0) \ll 1$ holds for all curves. That is, the criterion (2), which ensures complete passage of the generation current through the wide-bandgap layer of α-Si:H, also implies the smallness of $y_{SC}(0)$ in the short-circuit regime. We also note that if the coefficients θ_p and θ_n and the densities $n_0(d)$ and $p_0(0)$ are comparable, then, as calculations show, the criterion $\Delta y_{SC}(0) \ll 1$ also implies that $-\Delta y_{SC}(d) \ll 1$.

In the open-circuit regime, the relations (1) and (A1) allow one to find the respective dimensionless potentials at $x = 0$ and $x = d$ as

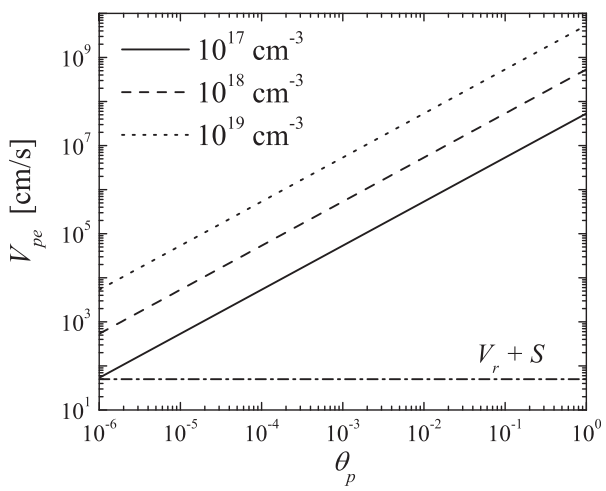

FIG. 8. Theoretical dependence of V_{pe} on θ_p in the highest-power regime.

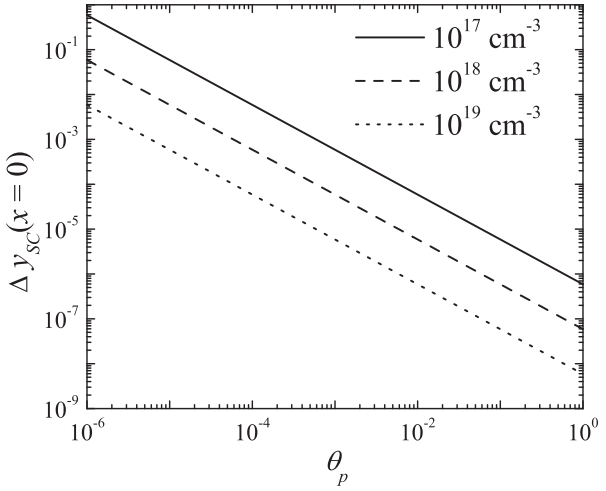

FIG. 9. Theoretical dependence of $\Delta y_{SC}(x = 0)$ on θ_p.

$$\Delta y_{OC}(0) = y(0) - y_0(0) = \ln\frac{p_0 + \Delta p_0}{p_0},$$
$$\Delta y_{OC}(d) = y(d) - y_0(d) = -\ln\frac{n_0 + \Delta p_0}{n_0}, \qquad \text{(A5)}$$

where Δp_0 is the excess electron–hole pair density in the open-circuit regime, with $\Delta p_0 \gg n_0, p_0$. Substitution of these expressions into Eq. (6) yields the result (7).

[1]W. G. J. H. M. van Sark, L. Korte, and F. Roca, *Physics and Technology of Amorphous-Crystalline Heterostructure Silicon Solar Cells* (Springer, Berlin, 2012).
[2]S. De Wolf, A. Descoeudres, Z. C. Holman, and C. Balif, Green **2**, 7 (2012).
[3]K. Masuko, M. Shigematsu, T. Hashiguchi, D. Fujishima, M. Kai, N. Yoshimura, T. Yamaguchi, Y. Ichihashi, T. Mishima, N. Matsubara, T. Yamanishi, T. Takahama, M. Taguchi, E. Maruyama, and S. Okamoto, IEEE J. Photovoltaics **4**, 1433 (2014).
[4]W. Shockley and H. J. Queisser, J. Appl. Phys. **32**, 510 (1961).
[5]A. Richter, M. Hermle, and S. W. Glunz, IEEE J. Photovoltaics **3**, 1184 (2013).
[6]D. Suwito, U. Jäger, J. Benick, S. Janz, M. Hermle, and S. W. Glunz, IEEE Trans. Electron Devices **57**, 2032 (2010).
[7]J. P. Seif, A. Descoeudres, M. Filipič, F. Smole, M. Topič, Z. C. Holman, S. De Wolf, and C. Ballif, J. Appl. Phys. **115**, 024502 (2014).
[8]A. Ya. Vul' and A. V. Sachenko, Sov. Phys. Semicond. **17**, 865 (1983).
[9]M. Taguchi, E. Maruyama, and M. Tanaka, Jpn. J. Appl. Phys., Part 1 **47**, 814 (2008).
[10]J. P. Seif, G. Krishnamani, B. Demaurex, Ch. Ballif, and S. De Wolf, IEEE J. Photovoltaics **5**, 718 (2015).
[11]M. W. M. van Cleef, M. W. H. Philippens, F. A. Rubinellia, M. Koltera, and R. E. I. Schroppa, MRS Proc. **420**, 239 (1996).
[12]T. F. Schulze, L. Korte, E. Conrad, M. Schmidt, and B. Rech, J. Appl. Phys. **107**, 023711 (2010).
[13]N. Dwivedi, S. Kumar, A. Bisht, K. Patel, and S. Sudhakar, Sol. Energy **88**, 31 (2013).
[14]X. Wen, X. Zeng, W. Liao, Q. Lei, and S. Yin, Sol. Energy **96**, 168 (2013).
[15]M. H. Vishkasougheh and B. Tunaboylu, Energy Convers. Manage. **72**, 141 (2013).
[16]E. Skoplaki and J. A. Palyvos, Sol. Energy **83**, 614 (2009).
[17]T. Mishima, M. Taguchi, H. Sakata, and E. Maruyama, Sol. Energy Mater. Sol. Cells **95**, 18 (2011).
[18]S. Abolmasov, A. Abramov, D. Andronikov, K. Emtsev, G. Ivanov, I. Nyapshaev, D. Orekhov, A. Semenov, G. Shelopin, E. Terukov, B. Strahm, G. Wahli, P. Papet, T. Söderström, Y. Yao, T. Hengst, and G. Kekelidze, in *Proceedings of The 31st European Photovoltaic Solar Energy Conference And Exhibition, Hamburg, Germany* (2015), p. 1046.
[19]D. W. Spaderna and D. H. Navon, IEEE Trans. Electron Devices **25**, 1290 (1978).
[20]M. A. Green, J. Appl. Phys. **67**, 2944 (1990).
[21]A. Hangleiter and R. Häcker, Phys. Rev. Lett. **65**, 215 (1990).
[22]A. V. Sachenko, A. P. Gorban, V. P. Kostylev, and I. O. Sokolovskii, Semiconductors **41**, 281 (2007).
[23]A. V. Sachenko, A. I. Shkrebtii, R. M. Korkishko, V. P. Kostylyov, M. R. Kulish, I. O. Sokolovskyi, and M. Evstigneev, J. Phys. D: Appl. Phys. **48**, 455101 (2015).
[24]A. V. Sachenko, A. I. Shkrebtii, R. M. Korkishko, V. P. Kostylyov, N. R. Kulish, and I. O. Sokolovskyi, Semiconductors **49**, 264 (2015).
[25]S. M. Sze and K. K. Ng, *Physics of Semiconductor Devices*, 3rd ed. (John Wiley and Sons, 2007).
[26]C. R. Osterwald, S. Anevsky, K. Bücher, A. K. Barua, P. Chaudhuri, J. Dubard, K. Emery, B. Hansen, D. King, J. Metzdorf, F. Nagamine, R. Shimokawa, Y. X. Wang, T. Wittchen, W. Zaaiman, A. Zastrow, and J. Zhang, Prog. Photovoltaics: Res. Appl. **7**, 287 (1999).
[27]Yu. V. Kryuchenko, A. V. Sachenko, A. V. Bobyl, V. P. Kostylyov, E. I. Terukov, A. S. Abramov, E. V. Mal'chukov, and I. O. Sokolovskyi, Semiconductors **49**, 683 (2015).
[28]J. P. Donnelly and A. G. Milnes, Int. J. Electron. **20**, 295 (1966); Proc. IEE **113**, 1468 (1966).
[29]A. Jano, S. Tohoda, K. Matsuyama, Y. Nakamura, T. Nishiwaki, K. Fujita, M. Taguchi, and E. Maruyama, in *Proceedings of the 28th European Photovoltaic Solar Energy Conference and Exhibition* (2013), pp. 748–751.
[30]R. L. Anderson, Appl. Phys. Lett. **27**, 691 (1975).
[31]E. Yablonovitch, D. L. Allara, C. C. Cheng, and T. B. Bright, Phys. Rev. Lett. **57**, 249 (1986).
[32]A. V. Sachenko, Yu. V. Kryuchenko, V. P. Kostylyov, N. R. Kulish, I. O. Sokolovskyi, and A. I. Shkrebty, Semiconductors **48**, 675 (2014).
[33]R. G. Ross, Jr. and M. I. Smokler, "Flat-plate solar array project," in *Engineering Sciences and Reliability* (Jet Propulsion Laboratory, CalTech, Pasadena, 1986), Vol. 6.
[34]M. F. Dias-Aquado, J. Grinbaum, W. T. Fowler, and E. G. Lightsey, Proc. SPIE **6221**, 622109 (2006).
[35]A. A. Gutkin and V. E. Sedov, Sov. Phys. Semicond. **10**, 945 (1976).